
Journal of Mathematical Imaging and Vision 21: 5–26, 2004

The Monogenic Scale-Space: A Unifying Approach to Phase-Based Image Processing in Scale-Space

M. FELSBERG*
Department of Electrical Engineering, Linköping University
mfe@isy.liu.se

G. SOMMER†
Institute of Computer Science and Applied Mathematics, Christian-Albrechts-University of Kiel
gs@ks.informatik.uni-kiel.de

Abstract. In this paper we address the topics of scale-space and phase-based image processing in a unifying framework. In contrast to the common opinion, the Gaussian kernel is not the unique choice for a linear scale-space. Instead, we chose the Poisson kernel since it is closely related to the monogenic signal, a 2D generalization of the analytic signal, where the Riesz transform replaces the Hilbert transform. The Riesz transform itself yields the flux of the Poisson scale-space and the combination of flux and scale-space, the monogenic scale-space, provides the local features phase-vector and attenuation in scale-space. Under certain assumptions, the latter two again form a monogenic scale-space which gives deeper insight to low-level image processing. In particular, we discuss edge detection by a new approach to phase congruency and its relation to amplitude based methods, reconstruction from local amplitude and local phase, and the evaluation of the local frequency.

Keywords: Poisson kernel, scale-space, local phase, analytic signal, Riesz transform, monogenic signal

1. Introduction

Scale-space representation is a well established technique in image processing. Linear scale-space is commonly equated with the Gaussian kernel and the heat (diffusion) equation. Investigations on these two approaches have led to a huge number of refinements and algorithms which have proven to be sophisticated methods for various applications.

Phase-based signal processing is a powerful technique for the analysis of structure based on the approach of quadrature filters. Although quadrature filters make use of bandpass filters, and therefore they are related to scale-space, the theory of the analytic signal and the scale-space theory are unrelated and independent frameworks, yet.

1.1. Overview of the Paper

This paper addresses the topic of combining scale-space theory and phase-based signal processing. In order to obtain an appropriate common theoretic framework, a linear scale-space is introduced which is not based on the heat equation. We replace the Gaussian kernel with the Poisson kernel, which is related to the potential (Laplace) equation.

A standard derivation of the Gaussian scale-space is obtained by combining the continuity equation and Fick's law yielding the heat equation [49]. Following the same idea for the derivation of the potential equation instead, the continuity equation must be combined

*This work has been supported by German National Merit Foundation, by DFG Graduiertenkolleg No. 357 and by DFG Grant FE 583/1-1.
†This work has been supported by DFG Grant So-320-2-2 and EC Grant IST-2001-34220.

with the Riesz transform [11], a multi-dimensional generalization of the Hilbert transform [18]. Accordingly, the image flux, or figure flow, is no longer given by the gradient in the image plane, but by the Riesz transform of the image for each scale.

The combination of a 1D signal and its Hilbert transform is called the analytic signal [25]. The analytic signal is the basis for all kinds of approaches which make use of the local phase. Similarly, the combination of a 2D signal and its Riesz transform is called the monogenic signal [18]. Hence, combining the scale-space representation obtained from the potential equation and its figure flow yields a generalization of the analytic signal in scale-space. As a consequence, a powerful theoretic framework is derived, which can be used for various image processing tasks.

The paper is organized as follows. In Section 1.2 we give a brief overview on the axiomatic of linear scale-space.

In Section 2 we introduce the Poisson scale-space and verify if it fulfills the mentioned axiomatics (Section 2.1). In Section 2.2 we relate the Poisson kernel to the Laplace equation and derive certain identities. The topic of causality is treated in Section 2.3 and by considering further properties of the Poisson scale-space (Section 2.4), we conclude the second part.

Section 3 deals with the combination of scale-space and phase-based image processing. We start with differential phase congruency as a method for edge detection (Section 3.1). After recalling several facts about the relationship between attenuation and phase in 1D (Section 3.2), we establish a similar theorem for the 2D case in Section 3.3. Using these results, we relate phase-based and amplitude-based image processing methods on a theoretic level (Section 3.4).

The paper is concluded with some final remarks, the appendix, and the references.

1.2. Axiomatics of Linear Scale-Space

In the scale-space literature, there are a couple of papers referring to the Gaussian scale-space as *the only linear scale-space*, e.g. [1, 29, 37]. Different authors used different definitions of scale-space to avoid arbitrary smoothing kernels. However, most authors formulated constraints to reduce the information in the image with increasing scale, like non-creation of local extrema [51], causality and non-enhancement of local extrema [33, 52]. Later, new scale-space definitions basing on scale invariant semigroup theory [22, 42] became popular. One of the aims of these scale-space definitions was to minimize the number of axioms uniquely determining the Gaussian scale-space. These formal axiomatics were mostly formulated without explicitly using the idea of information reduction, i.e., the intention of modern scale-space theory differs slightly from the first definitions.

According to [50], however, such a scale-space axiomatic based on semigroups has already been published much earlier [29]. The axiomatic is based on the assumption that there is an observation transformation Φ which transforms an image[1] $f(\mathbf{x})$ ($\mathbf{x} = (x, y)^T \in \mathbb{R}^2$) into a blurred version of the image $f_s(\mathbf{x})$.[2] The observation transformation has the general form

$$f_s(\mathbf{x}) = \Phi(f(\mathbf{x}'), \mathbf{x}, s) = \int_{\mathbb{R}^2} \phi(f(\mathbf{x}'), \mathbf{x}, \mathbf{x}', s)\, d\mathbf{x}', \tag{1}$$

where $s \in \mathbb{R}^+$. If the observation transformation fulfills certain constrains, it establishes a *scale and rotation invariant linear scale-space*[3]:

Definition 1 (Scale and rotation invariant linear scale-space). An observation transformation defines a scale and rotation invariant linear scale-space if it fulfills the subsequent axioms:

A1. It is linear (w.r.t. multiplications).
A2. It is shift invariant.
A3. It fulfills the semigroup property.
A4. It is scale and rotation invariant.
A5. It preserves positivity.

According to [50] (respectively [31]) we specify the axioms more formal:

A1. means that $\Phi(\lambda f(\mathbf{x}'), \mathbf{x}, s) = \lambda \Phi(f(\mathbf{x}'), \mathbf{x}, s)$ for any $\lambda \in \mathbb{R}$.
A2. means that $\Phi(f(\mathbf{x}' - \mathbf{x}_0), \mathbf{x}, s) = \Phi(f(\mathbf{x}'), \mathbf{x} - \mathbf{x}_0, s)$ for any $\mathbf{x}_0 \in \mathbb{R}^2$.
A3. means that there exists a mapping $S : \mathbb{R}^+ \times \mathbb{R}^+ \to \mathbb{R}^+$ so that $\Phi(\Phi(f(\mathbf{x}''), \mathbf{x}', s_1), \mathbf{x}, s_2) = \Phi(f(\mathbf{x}''), \mathbf{x}, S(s_1, s_2))$ for any $s_1, s_2 \in \mathbb{R}^+$.
A4. means that there exists a mapping $T : \mathbb{R}^+ \times \mathbb{R}^+ \to \mathbb{R}^+$ so that $\Phi(f(a\mathbf{R}\mathbf{x}'), \mathbf{x}, s) = \Phi(f(\mathbf{x}'), a\mathbf{R}\mathbf{x}, T(s, a))$ for any $a \in \mathbb{R}^+$ and any $\mathbf{R} \in \mathrm{SO}(2)$.
A5. means that $\Phi(f(\mathbf{x}'), \mathbf{x}, s) > 0$ for any $f > 0$ and for any $s \in \mathbb{R}^+$.

Note that the axioms of Iijima do not relate the scale-space representation to the absolute values of the original signal, i.e., if Φ is a linear scale-space, $k\Phi$ ($k > 0$) is also a linear scale-space of the same signal. This ambiguity can only be resolved by adding another constraint, for instance requiring that the signal is continuously embedded in the scale-space (i.e., if the scale tends to zero, Φ tends to the original signal).

Besides the axiomatic of Iijima, a couple of further axiomatics appeared in the literature. In this paper we only consider some additional axioms to those above; for a more exhaustive overview we refer to [50]. For each axiom we give either the original reference or the name of the author (the original reference can be found in [50]). The different axioms refer either to the observation transformation (respectively the generating convolution kernel) or to the *image flux*. The image flux, or *figure flow*, is the vector field whose divergence compensates the change of the signal through scale, i.e., the flux and the scale-space representation are related by the continuity equation [49].

A6. The flux is given by the maximum loss of 'figure impression' (Iijima).
A7. The kernel must be separable (Otsu).
A8. The scale-space must fulfill the causality requirement, i.e., isophotes must be connected to the original signal [33].
A9. Isophotes in scale-space must be upwards convex [33]; local maxima should not enhance with scale [1, 39].[4]
A10. No new maxima should be created with increasing scale (only valid in 1D [1]).

Based upon the mentioned axiomatics of linear scale-space, the convolution with a Gaussian kernel can be used to create blurred versions of the original image. In order to speed up the calculation, the blurred versions of the image are subsampled, yielding a resolution pyramid [9, 24]. Instead of performing convolutions, one can implement scale-space filtering using the underlying partial differential equation, in case of Gaussian scale-space the heat equation. The advantage of this method is that it is also possible to implement a non-linear heat equation, i.e., having a shift variant operator. This leads to non-linear diffusion methods [10, 43]. A further enhancement is obtained by replacing the scalar-valued diffusivity with a tensor-valued diffusivity, yielding anisotropic diffusion methods [46, 48, 49]. However, all these refinements of linear scale-space are out of the scope of this paper. We rather focus on the linear case, showing that there is another linear scale-space which fulfills most of the mentioned axioms.

2. Another Linear Scale-Space

In this section we introduce a new[5] linear scale-space, the *Poisson scale-space*. We show that the Poisson scale-space fulfills some important axiomatics which have appeared in the literature so far and discuss its behavior concerning level crossings and local extrema.

2.1. The Poisson Scale-Space

The 2D *Poisson kernel* is given by [47]

$$p(\mathbf{x}; s) = \frac{s}{2\pi (s^2 + |\mathbf{x}|^2)^{3/2}}. \tag{2}$$

It can be considered as a two-dimensional generalization of the *Cauchy probability density function* [13], i.e., the probability density function of the spatial coordinate at which a line with random orientation (uniformly distributed) intersects a plane at distance s. Interpreting the line as a light-ray emerging from a point-source with uniform radiance, the Poisson kernel turns out to be the point spread function of a defocused idealized optical system [20].

The Poisson kernel establishes a linear, isotropic scale-space, since it fulfills the axiomatic from Section 1.2 (see also [11, 15]):

Theorem 1 (*Poisson scale-space*)**.** *The Poisson kernel* (2) *establishes a linear scale-space in the sense of Definition* 1.

In order to prove this theorem, we need the Fourier transform of the Poisson kernel. The 2D Fourier transform is denoted by

$$\mathcal{F}_2\{f\}(\boldsymbol{\xi}) = \iint_{\mathbb{R}^2} f(\mathbf{x}) \exp(-i 2\pi\, \boldsymbol{\xi} \cdot \mathbf{x})\, d\mathbf{x}$$

where $\boldsymbol{\xi} = (\xi, \eta)^T$ and $\mathbf{x} = (x, y)^T$.

Lemma 1. *The spectrum of the Poisson kernel* (2) *is given by*

$$\mathcal{F}_2\{p(\cdot; s)\}(\boldsymbol{\xi}) = \exp(-2\pi |\boldsymbol{\xi}| s). \tag{3}$$

Proof: See [15, 47]. □

In the following we use the abbreviation $P(\boldsymbol{\xi}; s) = \mathcal{F}_2\{p(\cdot; s)\}(\boldsymbol{\xi})$.

Proof of Theorem 1:

- The axioms A1 and A2 are trivially fulfilled since $p(\mathbf{x}; s)$ is an LSI operator, i.e., it is applied by means of convolutions.
- Axiom A3: We have

$$\begin{aligned} P(\boldsymbol{\xi}; s_1)P(\boldsymbol{\xi}; s_2) &= \exp(-2\pi|\boldsymbol{\xi}|s_1)\exp(-2\pi|\boldsymbol{\xi}|s_2) \\ &= \exp(-2\pi|\boldsymbol{\xi}|(s_1 + s_2)) \\ &= P(\boldsymbol{\xi}; s_1 + s_2), \end{aligned}$$

  and hence $S(s_1, s_2) = s_1 + s_2$. In the spatial domain, this corresponds to $p(\mathbf{x}; s_1) * p(\mathbf{x}; s_2) = p(\mathbf{x}; s_1 + s_2)$.
- Axiom A4: Since

$$\begin{aligned} p(a\mathbf{R}\mathbf{x}; s) &= \frac{s}{2\pi((a|\mathbf{R}\mathbf{x}|)^2 + s^2)^{3/2}} \\ &= \frac{1}{a^2}\frac{s/a}{2\pi(|\mathbf{x}|^2 + (s/a)^2)^{3/2}} \\ &= \frac{1}{a^2}p(\mathbf{x}; s/a), \end{aligned}$$

  the observation transformation is scale and rotation invariant:

$$\begin{aligned} &\Phi(f(a^{-1}\mathbf{R}^T\mathbf{x}'), \mathbf{x}, s) \\ &= \iint_{\mathbb{R}^2} f(a^{-1}\mathbf{R}^T\mathbf{x}')p(\mathbf{x} - \mathbf{x}'; s)\, d\mathbf{x}' \\ &\quad \text{substitute } \mathbf{x} = a\mathbf{R}\mathbf{t} \text{ and } \mathbf{x}' = a\mathbf{R}\mathbf{t}' \\ &= \iint_{\mathbb{R}^2} f(\mathbf{t}')p(a\mathbf{R}(\mathbf{t} - \mathbf{t}'); s)a^2\, d\mathbf{t}' \\ &= \iint_{\mathbb{R}^2} f(\mathbf{t}')p(\mathbf{t} - \mathbf{t}'; s/a)\, d\mathbf{t}' \\ &= \Phi(f(\mathbf{x}'), \mathbf{x}, s/a). \end{aligned}$$

  Hence $T(s, a) = s/a$.
- Axiom A5 is fulfilled since $p(\mathbf{x}; s) > 0$ for all $\mathbf{x} \in \mathbb{R}^2$ and all $s \geq 0$. □

The proof also holds for other dimensions than two, especially in the 1D case [15]. Hence, we have found a counterexample of the uniqueness proof in [29]. At this point one might ask if the proof of Iijima contains an error. The answer is yes–Iijima assumes implicitly that the frequency response of the scale-space kernel is continuously differentiable at the origin (see appendix).

The Poisson kernel (2) is closely related to the Laplace equation (or potential equation)

$$\begin{aligned} \Delta_3 u(x, y, s) = u_{xx}(x, y, s) + u_{yy}(x, y, s) \\ + u_{ss}(x, y, s) = 0. \end{aligned} \tag{4}$$

To make this point more evident, consider the *fundamental solution*[6] of the Laplace equation:

$$\varphi(x, y, s) = -\frac{1}{4\pi\sqrt{x^2 + y^2 + s^2}}, \tag{5}$$

i.e., $\Delta_3\varphi(x, y, s) = \delta_0(x, y, s) = \delta_0(x)\delta_0(y)\delta_0(s)$ where δ_0 is the Dirac impulse. The identity above can easily be checked using the divergence (Gauss) theorem. A scalar function $u(x, y, s)$ which fulfills the Laplace equation is called a harmonic function (harmonic potential). The gradient field of a harmonic function $\mathbf{f}(x, y, s) = \nabla_3 u(x, y, s)$ is known to be irrotational and divergence free:

$$\begin{aligned} \operatorname{curl}\mathbf{f}(x, y, s) &= \nabla_3 \times \mathbf{f}(x, y, s) = 0, \\ \operatorname{div}\mathbf{f}(x, y, s) &= \nabla_3 \cdot \mathbf{f}(x, y, s) = 0 \end{aligned} \tag{6}$$

where $\nabla_3 = (\partial_x, \partial_y, \partial_s)^T$ is the 3D gradient operator. This system of equations formulates an equivalent problem to the one in (4) (up to an additive constant). Furthermore, since $\varphi(x, y, s)$ is the fundamental solution of the Laplace equation, $\nabla_3\varphi(x, y, s)$ is the fundamental solution of the system of equations in (6). This can easily be concluded by plugging $\nabla_3\varphi(x, y, s)$ into (6): $\nabla_3 \times \nabla_3\varphi \equiv 0$ and $\nabla_3 \cdot \nabla_3\varphi = \Delta_3\varphi$. Considering the components of $\nabla_3\varphi(x, y, s)$ yields

$$\begin{aligned} \partial_x\varphi(x, y, s) &= \frac{x}{4\pi(x^2 + y^2 + s^2)^{3/2}} \\ \partial_y\varphi(x, y, s) &= \frac{y}{4\pi(x^2 + y^2 + s^2)^{3/2}}, \\ \partial_s\varphi(x, y, s) &= \frac{s}{4\pi(x^2 + y^2 + s^2)^{3/2}} \end{aligned} \tag{7}$$

i.e., the Poisson kernel is one component of the fundamental solution of (6) (up to a factor of two).

Returning to the original setting of scale-space representation, the considered problem is a boundary value problem on the half-space $s > 0$. The appropriate method to get the solution of such a problem is the Schwarz reflection principle, which leads to a factor of two in the fundamental solution (see e.g. [7], p. 279).

Hence, the Poisson kernel is one component of the fundamental solution of (6) in the half-space $s > 0$.

2.2. *The Analytic and Monogenic Scale-Space Representations*

In image processing it is common to separate the image plane coordinates from the scale coordinate. Hence, we rewrite $\mathbf{f}(x, y, s) = (\mathbf{v}^T(\mathbf{x}; s), u(\mathbf{x}; s))^T$, i.e., $\mathbf{v}(\mathbf{x}; s)$ is a vector field $\mathbb{R}^2 \oplus \mathbb{R}^+ \to \mathbb{R}^2$, and we obtain a new set of equation from (6):

$$\operatorname{curl} \mathbf{v}(\mathbf{x}; s) = 0 \tag{8}$$

$$\nabla_2 \cdot \mathbf{v}(\mathbf{x}; s) + \partial_s u(\mathbf{x}; s) = 0 \tag{9}$$

$$\partial_s \mathbf{v}(\mathbf{x}; s) - \nabla_2 u(\mathbf{x}; s) = 0 \tag{10}$$

for all $s > 0$ and $\nabla_2 = (\partial_x, \partial_y)^T$. Obviously, the zero divergence in (6) yields the 2D continuity equation (9) which is also referred to in case of the Gaussian scale-space.

To obtain the Gaussian scale-space, the continuity equation (9) is combined with a figure flow according to Fick's law [49] or the maximum loss of figure impression (axiom A6) [50]. Fick's law basically says that the flux is proportional to the negative gradient, $\mathbf{v} = -k\nabla u$, $k > 0$. Hence, in context of images, the flux according to Fick's law is aiming the maximum reduction of gradients. Gradients, however, are considered to create the figure impression, i.e., Fick's law is equivalent to maximum loss of figure impression.

In the current framework, however, the figure flow is replaced with a flux $\mathbf{v}(\mathbf{x}; s)$ implicitly determined by (8)[7] and (10). The explicit solution is given by the *Riesz transform* [12, 47], a 2D generalization of the Hilbert transform [18], of u

$$\mathbf{v}(\mathbf{x}; s) = (\mathbf{h} * u(\cdot; s))(\mathbf{x}) \tag{11}$$

where the (vector-valued) kernel of the Riesz transform reads [47] (see also (7))

$$\mathbf{h}(\mathbf{x}) = \begin{pmatrix} h_1(\mathbf{x}) \\ h_2(\mathbf{x}) \end{pmatrix} = \frac{\mathbf{x}}{2\pi |\mathbf{x}|^3}. \tag{12}$$

Verifying that (11) is the appropriate figure flow of the Poisson scale-space representation u is much easier in the Fourier domain. The (vector-valued) frequency response of the Riesz transform is obtained as [47]

$$\mathbf{H}(\boldsymbol{\xi}) = -i\frac{\boldsymbol{\xi}}{|\boldsymbol{\xi}|}, \tag{13}$$

such that

$$\begin{aligned}
\mathcal{F}_2\{\operatorname{curl} \mathbf{v}(\cdot; s)\} &= i2\pi\xi i\frac{\eta}{|\boldsymbol{\xi}|}U(\boldsymbol{\xi}; s) \\
&\quad - i2\pi\eta i\frac{\xi}{|\boldsymbol{\xi}|}U(\boldsymbol{\xi}; s) = 0 \\
\mathcal{F}_2\{\nabla_2 \cdot \mathbf{v}(\cdot; s) + \partial_s u(\cdot; s)\} &= -i2\pi\xi i\frac{\xi}{|\boldsymbol{\xi}|}U(\boldsymbol{\xi}; s) \\
&\quad - i2\pi\eta i\frac{\eta}{|\boldsymbol{\xi}|}U(\boldsymbol{\xi}; s) \\
&\quad - 2\pi|\boldsymbol{\xi}|U(\boldsymbol{\xi}; s) = 0 \\
\mathcal{F}_2\{\partial_s \mathbf{v}(\cdot; s) - \nabla_2 u(\cdot; s)\} &= 2\pi|\boldsymbol{\xi}|i\frac{\boldsymbol{\xi}}{|\boldsymbol{\xi}|}U(\boldsymbol{\xi}; s) \\
&\quad - i2\pi\boldsymbol{\xi}U(\boldsymbol{\xi}; s) = 0,
\end{aligned}$$

where $U(\boldsymbol{\xi}; s) = \mathcal{F}_2\{u(\cdot; s)\}$. Note that similar to the gradient, the figure flow (11) can be used to define the *local orientation* of a signal [18].

The combination of a signal with its Riesz transform forms a 2D generalization of the analytic signal, the *monogenic signal* [18]:

$$\mathbf{f}_{\mathrm{M}}(\mathbf{x}) = \begin{pmatrix} (\mathbf{h} * f)(\mathbf{x}) \\ f(\mathbf{x}) \end{pmatrix} = \begin{pmatrix} (h_1 * f)(\mathbf{x}) \\ (h_2 * f)(\mathbf{x}) \\ f(\mathbf{x}) \end{pmatrix}. \tag{14}$$

The monogenic signal can be considered as a generalization of the analytic signal,[8] preserving a couple of properties of the latter:

- It consists of a combination of the original signal with a filtered version of itself, where the applied filter is odd and has an allpass amplitude response
- Its energy is twice the energy of the original signal.
- Local amplitude and local phase (-vector) can be extracted (see below).
- The monogenic signal of a harmonic oscillation (sine) contains a constant local amplitude and a linear local phase (modulo 2π).

Additionally, the monogenic signal is rotation invariant (it commutes with the rotation operator) and contains the local orientation information. For a more detailed discussion on the monogenic signal, refer to [15, 18].

Thus, using the Poisson kernel for generating a linear scale-space arises from combining the Riesz transform (12) with the continuity equation (9). The unique advantage of the Poisson scale-space compared to all other scale-spaces according to [42] (including the Gaussian scale-space) is the figure flow being in quadrature relation to the image at each scale. Hence, *local phase and local amplitude become inherent features of scale-space theory*. In order to understand the impact of this result to image processing, we consider the (better known) 1D case.

Defining the Poisson scale-space representation of a 1D signal using the same frequency response (3) as in the 2D case, the corresponding flux is given by the Hilbert transform of the signal at each scale. Combining the signal and its flux to a complex signal at each scale, yields a complex scale-space representation. This complex scale-space is the Poisson scale-space representation of the analytic signal.

Definition 2 (Analytic Poisson scale-space). The Poisson scale-space representation of a 1D analytic signal is called the 1D analytic Poisson scale-space representation.

The term 'analytic' is justified in a double sense. First, by definition the analytic Poisson scale-space is the Poisson scale-space representation of the *analytic* signal. Second, the analytic Poisson scale-space is an *analytic* function in the upper half-plane, i.e., it fulfills the Cauchy-Riemann equations, which is straightforward to verify. Since the Poisson scale-space is the only scale-space where signal and flux form an analytic signal, we use the term 'analytic scale-space' instead of 'analytic Poisson scale-space' in the sequel. Furthermore, since both components of an analytic function are harmonic [35], the Poisson scale-space might also be denoted *harmonic scale-space* and its flux might be denoted *conjugate harmonic scale-space*.

Similar to the 1D case, we define the corresponding 2D concept.

Definition 3 (Monogenic Poisson scale-space). The Poisson scale-space representation of a 2D monogenic signal is called the 2D monogenic Poisson scale-space representation.

As explained further above, the 2D monogenic scale-space representation is formed by the 2D Poisson scale-space representation of a signal and the corresponding figure flow. It is a *monogenic* function in the upper half-space $s > 0$. Monogenic functions are solutions of the generalized Cauchy-Riemann equations, known from Clifford analysis [5]. Since we only consider (para-)vector valued functions, the here considered monogenic functions are equivalent to 3D vector fields with zero divergence and zero curl, and the generalized CRE are equivalent to (6).[9] Hence, the term 'monogenic' in Definition 3 is also justified for two reasons: First, by definition it is the Poisson scale-space representation of the monogenic signal. Second, it is monogenic for $s > 0$. Again, the Poisson framework is the only one yielding monogenic functions, so that we use the term 'monogenic scale-space' for the scale-space defined in Definition 3. Similar as in the 1D case, all components of a monogenic function are harmonic [15], and hence one might use 'harmonic scale-space' instead of Poisson scale-space and 'conjugate harmonic scale-space' for the corresponding flux. An overview of the concept of monogenic scale-space is given in Fig. 1.

2.3. Relaxed Causality

The causality of scale-space representation (axiom A8) was introduced in [33] as a fundamental concept. Therein causality is defined by the statement: 'any feature at a coarse level of resolution is required to possess a (not necessarily unique) "cause" at a finer level of resolution although the reverse need not be true.' The subsequent formal treatment however, is slightly stricter, and it requires that the convex side of an isophote in an extremum points towards coarser scales (axiom A9). Hence, this requirement is equivalent to the non-enhancement of local extrema [1, 39].

For continuous[10] signals, the non-enhancement property is only fulfilled in the case of the Gaussian scale-space [1], and therefore the Poisson scale-space does not fulfill the causality requirement in its stricter formulation, see also Fig. 2. However, motivated by the relationship between causality and the maximum principle [28],[11] we use the original informal definition of causality to prove that the Poisson scale-space is causal in a relaxed sense.

Definition 4 (relaxed causality). A scale-space representation $u(\mathbf{x}; s)$ is called causal in a relaxed sense, if any level crossing surface, i.e., any connected component of $u(\mathbf{x}; s) = \lambda$, $\lambda \in \mathbb{R}$, is connected to a point $u(\mathbf{x}; 0) = \lambda$.

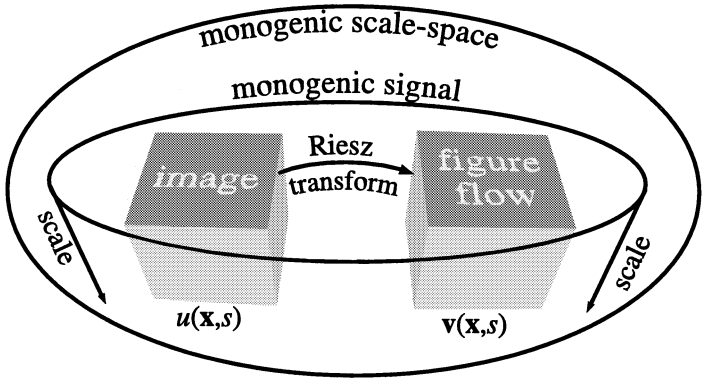

Figure 1. Relations between Riesz transform, monogenic signal, Poisson scale-space, and monogenic scale-space. The Riesz transform of an image at an arbitrary scale yields the corresponding figure flow. The image and its figure flow form a monogenic signal. The monogenic signals at all scales build up the monogenic scale-space. Alternatively, the Poisson scale-space is obtained from the original image by Poisson filtering. Computing the harmonic conjugate yields the corresponding figure flow at all scales. The Poisson scale-space and its harmonic conjugate form the monogenic scale-space.

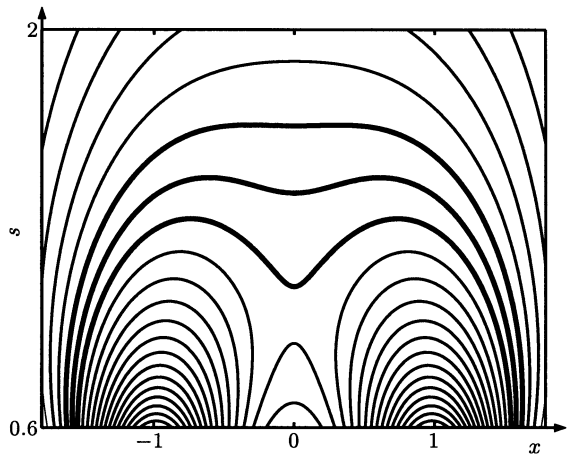

Figure 2. Example due to [1] (three Dirac impulses with unit distance; the weights of the outer ones are 25 times larger than the weight of the center one), showing that the 1D Poisson scale-space does not fulfill the non-enhancement axiom A9.

Relaxing the causality requirement enables us to categorize the Poisson scale-space to be causal although it does not fulfill the non-enhancement property.

Theorem 2 (*relaxed causality of Poisson scale-space*)**.** *The Poisson scale-space representation of a* 2*D signal in* $\mathbb{L}_1$ *fulfills the relaxed causality requirement according to Definition* 4*.*

Proof: The proof consists of two parts. First, we show that there exists no closed level crossing surface for nontrivial signals and $s > 0$. Second, we show that any open level crossing surface intersects the plane $s = 0$. The Poisson scale-space representation is denoted by $u(\mathbf{x}; s)$.

Assume that there exists a closed level crossing surface c_λ given by a connected component of $u(\mathbf{x}; s) = \lambda$, $\lambda \in \mathbb{R}$ and $s > 0$. Due to the maximum principle of harmonic functions [35], i.e., harmonic functions take their maximum and minimum on the boundary, we know that $u(\mathbf{x}; s) = \lambda$ everywhere inside of c_λ. Since the Poisson kernel is differentiable for $s > 0$, $u(\mathbf{x}; s)$ is also differentiable for $s > 0$. Hence, either $u(\mathbf{x}; s)$ is constant (and therefore zero, since it is in $\mathbb{L}_1$) or there exists an $\varepsilon \neq 0$ such that the connected component $c_{\lambda+\varepsilon}$ of $u(\mathbf{x}; s) = \lambda + \varepsilon$ is a level crossings which lies entirely outside the level crossing c_λ (see Fig. 3). Making use of the maximum principle once more, we know that $u(\mathbf{x}; s) = \lambda + \varepsilon$ everywhere inside of $c_{\lambda+\varepsilon}$ which yields a contradiction.

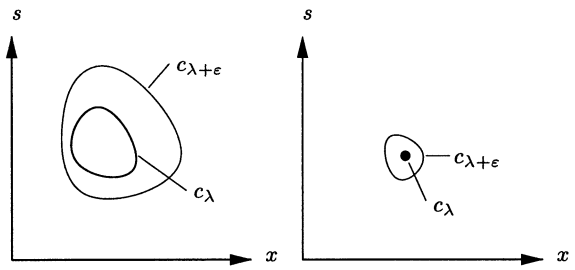

Figure 3. Level crossings at the levels λ and $\lambda + \varepsilon$ illustrating the argumentation in the proof of Theorem 2.

Knowing that all level crossings must be open, we just have to show that each of them is connected to the plane $s=0$. Since both the original signal and the Poisson kernel are in $\mathbb{L}_1$, $u(\mathbf{x};s)$ is in $\mathbb{L}_1$ for each $s \geq 0$, too. Hence, $\lim_{|\mathbf{x}|\to\infty} u(\mathbf{x};s)=0$ for each $s \geq 0$. Furthermore, $\lim_{s\to\infty} p(\mathbf{x};s)\equiv 0$, and hence $\lim_{s\to\infty} u(\mathbf{x};s)\equiv 0$. Thus all level-crossings with $\lambda \neq 0$ are connected to the plane $s = 0$. There might exist zero-crossings which are connected to the planes given by $s \to \infty$ and $|\mathbf{x}| \to \infty$, but these planes are connected to each other and especially to the line given by $|\mathbf{x}| \to \infty$ and $s=0$, which is part of the plane $s=0$. □

The nice thing about relaxed causality is that under certain assumptions it is also fulfilled by the absolute value $\sqrt{u(\mathbf{x};s)^2 + |\mathbf{v}(\mathbf{x};s)|^2}$ of the monogenic scale-space:

Theorem 3 (*relaxed causality of monogenic scale-space*)**.** *The absolute value of the monogenic scale-space representation of a* 2*D signal in* $\mathbb{L}_1$ *fulfills the relaxed causality requirement according to Definition* 4 *if the monogenic scale-space representation contains no zeros.*

The proof is basically the same as for Theorem 2. Instead of using the maximum principle for harmonic functions, the maximum principle of monogenic functions is applied [27]. To assure that no local minimum occurs, one has to exclude zeros in the upper half-space (in analogy to [8], p. 364).

In order to illustrate the two different definitions of causality, we switch to 1D scale-space. In Fig. 4 four different cases of isophotes are illustrated.

According to the two different definitions of causality, we obtain the following categorization:

1. The isophote is closed for $s > 0$. We do not have causality in the strict sense, since the convex side also points towards finer scales. We also do not have causality in the relaxed sense, since the surface is not connected to a point on the line $s = 0$.
2. The isophote is connected to the line $s = 0$ and it is convex w.r.t. increasing scale. Hence, we have causality according to both definitions.
3. The isophote is connected to the line $s = 0$ but it is not convex w.r.t. increasing scale for all x, it is concave at the point P. In this case we only have causality in the relaxed sense.
4. The isophote is not closed and not connected to the line $s = 0$. We do not have strict causality since the surface is concave. We do not have relaxed causality either since the surface is not connected to the line $s = 0$.

Actually, there are other possible cases like open surfaces which intersect the line $s = 0$ in only one point, but those are not relevant for the current discussion. The main difference between the two definitions of causality boils down to the third case. Whereas strict causality requires the isophote to be connected to the plane $s = 0$ in the space 'between' the current scale and scale zero, the relaxed causality only requires connectivity in the whole half-space $s > 0$.

At this point a discussion of the decisive difference of the two definitions is necessary. Before we go into details, we have to mention that the difference is of a rather theoretic nature. In practice, i.e., with a sampled scale axis, the third case in Fig. 4 is hardly observable at all, since the 'deepness' of the concave area (if it occurs at all) is very limited. This observation brings us to the first point of theoretic interest: Is it possible to find an $\varepsilon > 0$, such that the connected component lives in $\mathbb{R}^2 \times [0, s_0 + \varepsilon)$ if the local extremum occurs at scale s_0. This question is also fundamental to practical problems, since it might give a rule of thumb for scale-ranges of isophote tracking.

A first rough upper bound to ε is obtained by looking at the spatial global maximum (isophote level $\lambda > 0$)

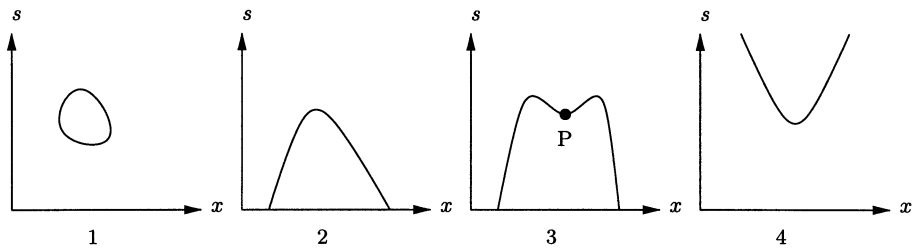

Figure 4. Causality vs. relaxed causality in 1D scale-space. The two definitions only differ with respect to the third case.

or minimum ($\lambda < 0$) with the same value λ as the isophote. Assume this maximum (minimum) occurs at scale s_1. Due to the maximum principle, $u(\mathbf{x}; s)$ takes smaller (larger) values for $s > s_1$ and hence, $\varepsilon < s_1 - s_0$. From this observation, we conclude that

- for global maxima and minima (in the image plane) the non-enhancement property is fulfilled
- and the expected value of ε decreases with increasing $|\lambda|$.

However, finding a tighter bound for ε turns out to be quite hard.

A main argument for the causality principle is to avoid the creation of spurious structures [33]. On a purely theoretic level, this is equivalent to the non-enhancement property. In practice, however, one should take into account that signals contain noise and are quantized. Hence, a spurious structure only becomes visible if its intensity is sufficiently high to supersede the noise and to reach the next quantization level. Indeed, the spurious structures created by the Poisson filtering are typically of a very low relative dynamics compared to the neighbored structure which causes it. Due to noise and quantization effects the created structures therefore become invisible. Take for instance the signal which was used to create Fig. 2. The weights of the impulses are chosen, such that the enhancement of the maximum at $x = 0$ becomes clearly visible. On a quantized gray level image (256 gray levels, the height of the outer impulses correspond to the full range), there is exactly one observable enhancement step of the maximum by one gray level, i.e., in the presence of noise, no enhancement would be observable.

2.4. *Further Properties*

In this section, we compare the Poisson scale-space to the Gaussian scale-space with respect to several properties.

Same as in the Gaussian scale-space, the original image is continuously embedded in its Poisson scale-space, which follows from the subsequent lemma.

Lemma 2. *If s tends to zero, $p(\mathbf{x}; s)$ tends to a 2D Dirac delta function, i.e.,* $\lim_{s\to 0} p(\mathbf{x}; s) = \delta_0(\mathbf{x})$, *where* $\delta_0(\mathbf{x}) = \delta_0(x)\delta_0(y)$.

Proof: One possible definition of the 1D Dirac delta function is

$$\delta_0(x) = \begin{cases} 0 & \text{if } x \neq 0 \\ \infty & \text{if } x = 0 \end{cases} \quad \text{and} \quad \int_{\mathbb{R}} \delta_0(x)\, dx = 1.$$

The 2D Dirac impulse is defined to be the product of the 1D Dirac impulses in x- and y-direction. Hence, the integral property changes to $\iint_{\mathbb{R}^2} \delta_0(\mathbf{x})\, d\mathbf{x} = 1$. If $s = 0$ and $\mathbf{x} \neq 0$ we have $p(\mathbf{x}; s) = 0$. For $s > 0$, $p(0; s) = (2\pi s^2)^{-1}$ so that $\lim_{s\to 0} p(0; s) = \infty$. Furthermore,

$$\iint_{\mathbb{R}^2} p(\mathbf{x}; s)\, d\mathbf{x} = \int_0^{2\pi} \int_0^{\pi/2} \frac{\sin\theta}{2\pi}\, d\theta\, d\psi = 1 \quad \text{for all } s > 0.$$

□

Lemma 2 is also reasonable from a probabilistic point of view and from a physical point of view (see Section 2.1).

The axioms A6, A8, and A9 have been intensively discussed in the previous two sections. The axiom A7 (separability) is obviously not fulfilled by the Poisson kernel, nor by any other scale-space kernel except for the Gaussian [11]. Separability is mostly required due to practical reasons, i.e., computational speed. Hence, the computation of the Poisson scale-space by convolutions is definitely slower than the computation of the Gaussian scale-space. For FFT-based implementations, both scale-spaces are equally fast to compute.

The last remaining axiom is the non-creation axiom (A10). However, it is well known that the non-creation of local extrema in 1D Gaussian scale-space does not generalize to higher dimensions [37]. Instead of considering the creation of local extrema, the authors in [1] consider (zero-crossing) contours, showing that these contours can merge and split with increasingly fine scale. We adapted their example of the 'dumbbell' (Fig. 5, left) to illustrate the corresponding property of the Poisson scale-space. Same as for the Gaussian case, the contours can split and merge, see Fig. 5, right.

Besides the axioms we have verified above, there are a pile of further axioms which are considered in the context of the Poisson kernel in [11, 12, 42]. Apart from the mentioned axioms, there are other interesting properties of the Gaussian scale-space which are now reviewed in context of the Poisson scale-space.

Like for the Gaussian scale-space, the Poisson scale-space representation can be used to interpret images in term of singularities, extrema, saddle-points, etc.

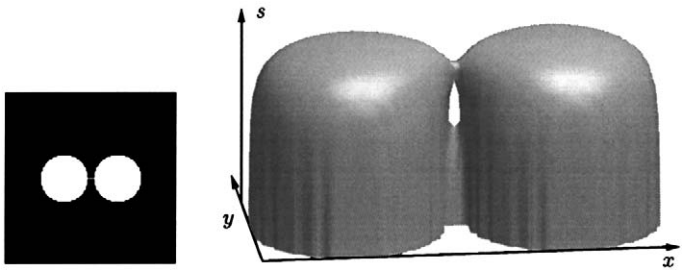

Figure 5. Test pattern from [1] (left) and a resulting level-crossing surface in scale-space (right).

(see [23, 33]). However, for the Poisson scale-space a new systematic evolves. The 1D Poisson scale-space is closely related to the Laplace transform [45] (and therefore to the Z-transform), which give rise to signal representation and interpretation in terms of zeros and poles. In Theorem 5 (see also [15]) it is shown that the spectrum of an analytic signal in the Poisson scale-space is given by the one-sided Laplace transform of the original spectrum. Hence, the zeros and poles in the spatial domain completely represent the original spectrum. Generalizing this idea to 2D, it is reasonable that the zero-crossings, singularities, and saddle-points in scale-space completely represent the original spectrum. However, the corresponding systematic for the 2D Poisson scale-space will be the topic of a future publication.

Besides the behavior of the signal in scale-space, it is also reasonable to compare the two involved convolution kernels. The Gaussian kernel is known to be the only real-valued operator with the optimal uncertainty of $(2\pi)^{-1}$, [3, 41]. The uncertainty of the Poisson kernel is just slightly worse (by a factor of $\sqrt{1.5}$, see appendix). This slight increase of uncertainty is caused by the larger extent of the Poisson kernel in both domains, see Fig. 6. For the sake of simplicity, the figure shows the comparison for the 1D case, but it is basically the same for 2D, see [15]. To compare both kernels, the maximum of the Poisson kernel is chosen to be the same as the one of the Gaussian kernel ($s = \sqrt{2}\sigma/\sqrt{\pi}$ [15]).

The larger extent of the Poisson kernel in the spatial domain results in two effects. First, as a qualitative difference, the Poisson kernel leads to a violation of the non-enhancement property, see the discussion in the previous section. Second, as a quantitative difference, the truncation-error of the Gaussian kernel and the Poisson kernel differ, see Table 1. Compared to the Gaussian kernel, the $\mathbb{L}_1$-truncation error of the Poisson kernel is much higher, whereas the $\mathbb{L}_2$-truncation error is much lower for small filter masks.

The larger extent of the Poisson kernel in the frequency domain yields a different behavior for the bandlimitation, and therefore a different subsampling strategy if the Poisson kernel is applied for creating a

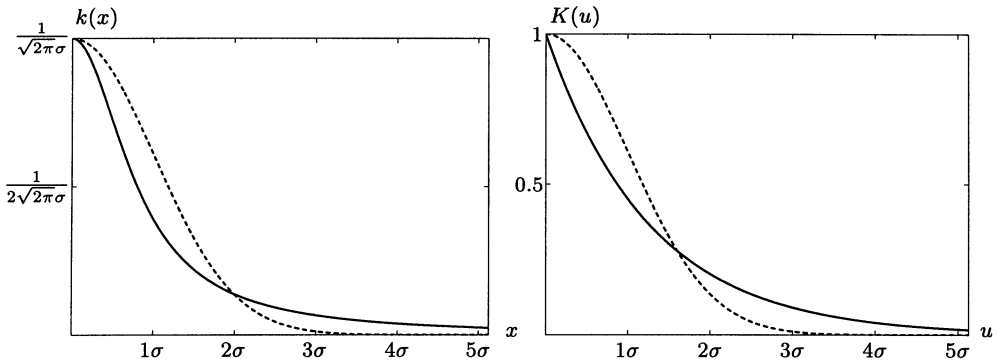

Figure 6. The 1D Gaussian kernel (dashed line) and the 1D Poisson kernel (solid line) in spatial domain (left) and frequency domain (right). All axes are labeled relative to the standard deviation σ of the Gaussian. The Poisson kernel is less rapidly decreasing than the Gaussian kernel, i.e., it has a larger extent.

Table 1. Truncation error of the 2D Gaussian kernel and the 2D Poisson kernel. The kernels are truncated at σ, 2σ, and 3σ ($s = \sigma$ [15]).

Truncation/error norm	$\sigma/\mathbb{L}_1$	$2\sigma/\mathbb{L}_1$	$3\sigma/\mathbb{L}_1$	$\sigma/\mathbb{L}_2$	$2\sigma/\mathbb{L}_2$	$3\sigma/\mathbb{L}_2$
Gaussian kernel	61%	14%	1%	37%	2%	0%
Poisson kernel	71%	45%	32%	25%	4%	1%

multi-resolution representation. The involved parameters and alias effects can easily be determined from the frequency response. However, this topic is out of the scope of this paper. Instead, we now focus on the relationship between the Poisson scale-space and phase-based image processing.

3. The Local Phase in Scale-Space

In the preceding sections of this paper, we have presented the Poisson scale-space as a possible alternative to the Gaussian scale-space. However, there are more alternatives [12] and it is legitimate to ask why to change existing methods using the Gaussian kernel. For many applications it is appropriate to keep with the Gaussian kernel, however, there are cases where it might be advantageous or even necessary to switch to the Poisson scale-space. One of the latter cases arises if the ideas of local phase and scale-space are combined to recognize local structures and to measure local features. The direct relationship between the Poisson scale-space and the monogenic signal (see Section 2.2) yields new possibilities of phase-based image processing in scale-space. To show the advantages of a common framework, we start with a simple application: edge detection by differential phase congruency. In the subsequent sections, we derive a 2D generalization of the attenuation-phase relationship based upon intrinsically 1D monogenic signals. The aim of this relationship is to understand the deeper connection between phase-based and amplitude-based approaches to edge detection and local frequency estimation (see last section).

3.1. Differential Phase Congruency

Edge detection by means of quadrature filters can be performed in two ways: either by detecting local maxima of the local amplitude or by detecting points of stationary phase in scale-space. The latter approach is commonly called *phase congruency* and is based on comparisons of the local phase at certain distinct scales [34, 44]. There are basically three drawbacks of using distinct scales:

- Edges are scale-relative, i.e., they have a certain optimal scale for detection and have a limited extent in scale-space. An algorithm using distinct scales has to contain some heuristics to judge whether an edge is present or not if the phase is only congruent in *some* of the considered scales.
- It is not straightforward, how to map at different scales estimated phases to a (scalar) certainty measure.
- Due to sampling of the orientation and of the scale, a large number of basis filters has to be applied, yielding a high computational complexity.

In [17] we presented a phase congruency based edge detector which makes use of the monogenic signal. Although that method is already much faster than the classical methods cited above, the drawbacks concerning the choice of scales and the evaluation of a certainty measure are still present. In [15] an advanced method has be developed based on the idea of *differential phase congruency*.

Before we consider the new approach more in detail, we must define the phase approach of the monogenic scale-space (see also [18]).

Definition 5 (local phase-vector). Let $u(\mathbf{x}; s)$ be a Poisson scale-space representation and $\mathbf{v}(\mathbf{x}; s)$ its harmonic conjugate. Then, the local phase-vector of the monogenic scale-space representation $(\mathbf{v}^T, u)^T$ is defined by

$$\mathbf{r}(\mathbf{x}; s) = \frac{\mathbf{v}(\mathbf{x}; s)}{|\mathbf{v}(\mathbf{x}; s)|} \arctan\left(\frac{|\mathbf{v}(\mathbf{x}; s)|}{u(\mathbf{x}; s)}\right), \qquad (15)$$

where $\arctan(\cdot) \in [0, \pi)$.

The idea behind this definition is to create a combined representation of local phase and local orientation, as it is proposed in [25], p. 274. The local phase and the local orientation define a point on the unit sphere. Every point on the unit sphere can be mapped one-to-one to a rotation vector in the plane [15]. A rotation vector points into the direction of the rotation axis and its absolute value defines the rotation angle. The local phase-vector describes a rotation by the phase angle around an axis perpendicular to the local orientation.

Note that the phase-vector is parallel to the local orientation, and hence, perpendicular to the actual rotation axis.

The local phase-vector characterizes the local gray level transition of an image (i.e., the local image structure) completely, if the image is locally constant in one direction. In [25] these signals are called *simple* (local) signals. A more generic terminology in this context is the notion of the *local intrinsic dimension*, see e.g. [36].

Definition 6 (local intrinsic dimension). The local intrinsic dimension of an image neighborhood is given by the minimal number of orthogonal orientations in which the image locally varies.

Hence, lines and edges are typical examples for intrinsically 1D neighborhoods. In [18] we have shown, that for intrinsically 1D neighborhoods the phase angle contained in the phase-vector equals the local phase of the corresponding 1D signal. This also implies that the 2D phase congruency at lines and edges directly corresponds to the 1D phase congruency at impulses and steps.

The idea of differential phase congruency is now to replace the finite difference of phases on different scales by a scale derivative of the phase:

Definition 7 (differential phase congruency). Let $\mathbf{r}(\mathbf{x}; s)$ be the local phase-vector of a monogenic scale-space representation. Points where

$$\partial_s \mathbf{r}(\mathbf{x}; s) = 0 \tag{16}$$

are called points of differential phase congruency.

Using this definition does not yield an advantage compared to ordinary phase congruency according to [17], if the scale derivative has to be approximated with finite differences. However, since the monogenic scale-space unifies the frameworks of phase-based processing and scale-space, it is possible to derive a formula for computing the derivative directly.

The scale derivative of the local phase-vector can be computed as follows:

Theorem 4 (*scale derivative of phase-vector*)**.** *For intrinsically* 1*D neighborhoods the scale derivative of the local phase-vector of a monogenic scale-space representation*, $\mathbf{r}(\mathbf{x}; s)$, *is given by*

$$\partial_s \mathbf{r}(\mathbf{x}; s) = \frac{u(\mathbf{x}; s)\partial_s \mathbf{v}(\mathbf{x}; s) - \mathbf{v}(\mathbf{x}; s)\partial_s u(\mathbf{x}; s)}{u(\mathbf{x}; s)^2 + |\mathbf{v}(\mathbf{x}; s)|^2}. \tag{17}$$

Proof: The scale derivative of (15) reads

$$\partial_s \mathbf{r}(\mathbf{x}; s) = \arctan\left(\frac{|\mathbf{v}(\mathbf{x}; s)|}{u(\mathbf{x}; s)}\right)\partial_s \frac{\mathbf{v}(\mathbf{x}; s)}{|\mathbf{v}(\mathbf{x}; s)|} + \frac{\mathbf{v}(\mathbf{x}; s)}{|\mathbf{v}(\mathbf{x}; s)|}\,\partial_s \arctan\left(\frac{|\mathbf{v}(\mathbf{x}; s)|}{u(\mathbf{x}; s)}\right).$$

Since the neighborhood is intrinsically 1D, the local orientation does not change through scale, i.e., $\mathbf{v}/|\mathbf{v}|$ is constant, such that the first term vanishes. Rewriting $\mathbf{v}$ as $v\mathbf{n} = v(\cos\theta, \sin\theta)^T$ for appropriate θ and $v \geq 0$, the second term reads

$$\begin{aligned}
&\frac{\mathbf{v}(\mathbf{x}; s)}{|\mathbf{v}(\mathbf{x}; s)|}\,\partial_s \arctan\left(\frac{|\mathbf{v}(\mathbf{x}; s)|}{u(\mathbf{x}; s)}\right) \\
&= \mathbf{n}\,\partial_s \arctan\left(\frac{v(\mathbf{x}; s)}{u(\mathbf{x}; s)}\right) \\
&= \frac{\mathbf{n}(u(\mathbf{x}; s)\partial_s v(\mathbf{x}; s) - v(\mathbf{x}; s)\partial_s u(\mathbf{x}; s))}{u(\mathbf{x}; s)^2 + v(\mathbf{x}; s)^2} \\
&= \frac{u(\mathbf{x}; s)\partial_s \mathbf{v}(\mathbf{x}; s) - \mathbf{v}(\mathbf{x}; s)\partial_s u(\mathbf{x}; s)}{u(\mathbf{x}; s)^2 + |\mathbf{v}(\mathbf{x}; s)|^2}.
\end{aligned}$$

□

This formula is especially useful, since it yields a higher accuracy and a significant speedup of the derivative computation compared to a finite difference approximation. The scale derivative is obtained from six linear filters: the Poisson filter, its Riesz transform, and their scale derivatives. The phase congruency itself is obtained without using inverse trigonometric functions. An alternative to (17) would be to replace the s-derivatives of the kernels with $\mathbf{x}$-derivatives (see (9), (10), and Section 3.4).

Returning to the points of phase congruency, we have to find the zeros of the two components of the numerator in (17). By a linear regression, these zeros can easily be detected with subpixel accuracy. After removing those zeros where the slope of the numerator in (17) is smaller than a threshold, the results in Fig. 7 are obtained.

3.2. The Local Attenuation—Local Phase Relationship in 1D

The 1D attenuation-phase relationship (see e.g. [40], p. 206), states that for a minimum-phase system,[12] the attenuation (logarithm of the amplitude response) and the phase response are related by the Hilbert transform.

In order to explore the background of this relationship, we consider an analytic function $w(z)$ which is

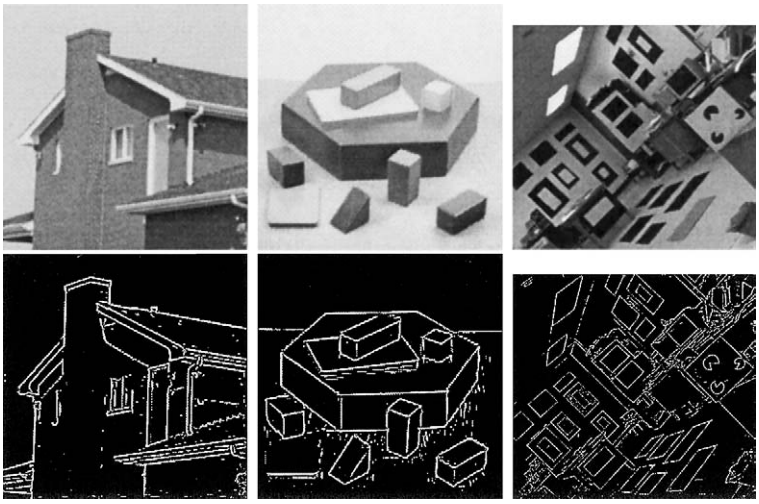

Figure 7. Results from differential phase congruency. Upper row: original images. Bottom row: detected edges and lines (same parameters for all images). For comparison, see [15].

non-zero everywhere. Hence, $\log(w(z))$ is also analytic and non-singular, which can easily be checked using the Cauchy-Riemann equations. Considering the Laplace transform of a causal system, its transfer function is analytic in the positive half-plane. Hence, attenuation and phase response form an analytic function in this half-plane if the filter is minimum-phase and therefore, attenuation and phase response form a Hilbert pair on each line $\mathrm{Re}\{z\} > 0$.

The idea of the attenuation-phase relationship can be transferred to the analytic scale-space representation, since the latter equals the Laplace transform [45] if the roles of Fourier domain and spatial domain are exchanged [15].

Theorem 5 (*analytic scale-space and Laplace transform*). *Let $u(x;s) + iv(x;s)$ be the analytic scale-space representation of a $1D$ signal $f(x)$. Then,*

$$u(x;s) + iv(x;s) = 2\mathcal{L}\{F\}(2\pi(s - ix)), \qquad (18)$$

where $F = \mathcal{F}_1\{f\}$ and $\mathcal{L}$ denotes the Laplace transform

$$\mathcal{L}\{g\}(p) = \int_0^\infty \exp(-px)g(x)\,dx \qquad (19)$$

with $p \in \mathbb{C}$ and $\mathrm{Re}\{p\} > 0$.

Proof: Starting from the right and plugging in the frequency response of the Hilbert transform $-iu/|u|$ yields

$$\begin{aligned}
&2\mathcal{L}\{F\}(2\pi(s - ix)) \\
&= 2\int_0^\infty \exp(-(2\pi(s - ix))u)F(u)\,du \\
&= 2\int_0^\infty F(u)\exp(-2\pi|u|s)\exp(i2\pi xu)\,du \\
&= \int_{-\infty}^\infty \left(1 + \frac{u}{|u|}\right)F(u)\exp(-2\pi|u|s)\exp(i2\pi xu)\,du \\
&= u(x;s) + iv(x;s).
\end{aligned}$$

□

Hence, we can apply the attenuation-phase relationship of minimum phase systems to 1D analytic scale-space representations which are non-zero everywhere.[13] Instead of phase and attenuation, the *local* phase and the *local* attenuation now form a Hilbert pair for each scale. The local attenuation is simply the logarithm of the local amplitude. Unfortunately, analytic scale-space representations often contain zeros for $s > 0$, see e.g. Fig. 8.

Zeros typically occur if a signal contains a high frequency component with a higher amplitude than a low frequency component. Descending through scale-space, the amplitude of the low frequency component will eventually be larger. Thus the number of modes changes and the zero crossings intersect, see Fig. 9.

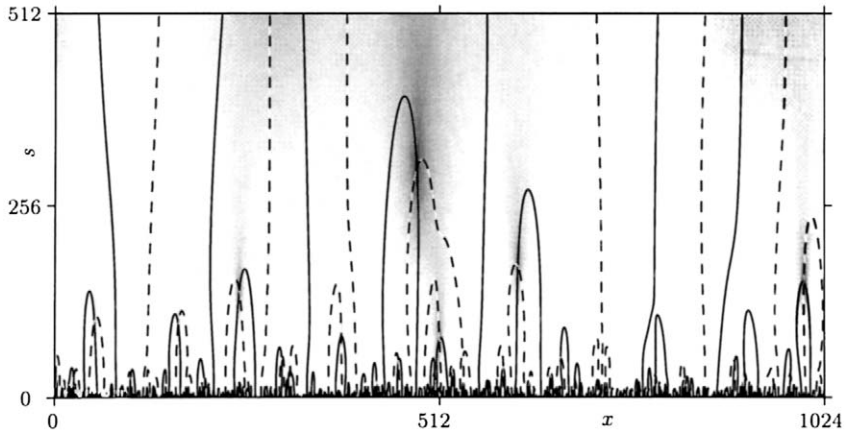

Figure 8. 1D Poisson scale-space: zeros of the local amplitude of a random signal. The zero-crossings of the real part are indicated by solid lines, the zero-crossings of the imaginary part are indicated by dashed lines. The gray level image in the background shows the (rescaled) local amplitude. Note that a zero of the local amplitude implies both parts, the real one and the imaginary one, to be zero.

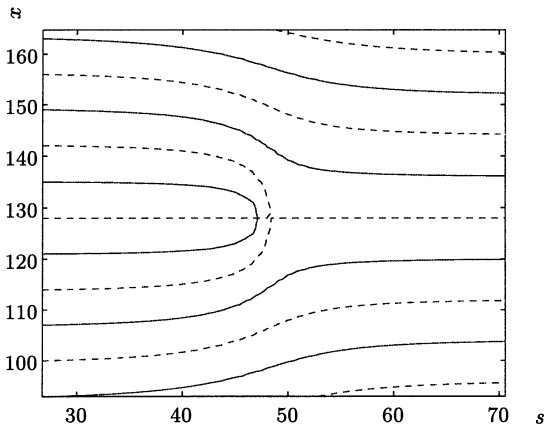

Figure 9. Intersecting zeros of real part (solid line) and imaginary part (dashed line) for a simple linear combination of two oscillations.

3.3. The Local Attenuation—Local Phase Relationship in 2D

In this section we generalize the relationship between local attenuation and local phase for the 2D case, i.e., the monogenic signal.

For the 2D monogenic signal, the local phase is replaced with a phase-vector, see (15). The local amplitude is given by the $\mathbb{L}_2$-norm of the vector $(\mathbf{v}^T, u)^T$ at every point $(\mathbf{x}; s)$ [18] and hence, the 2D local attenuation is given by

$$\begin{aligned} a(\mathbf{x}; s) &= \log(\sqrt{u(\mathbf{x}; s)^2 + |\mathbf{v}(\mathbf{x}; s)|^2}) \\ &= \frac{1}{2}\log(u(\mathbf{x}; s)^2 + |\mathbf{v}(\mathbf{x}; s)|^2). \end{aligned} \tag{20}$$

Under certain assumptions, local phase-vector and local attenuation form a Riesz triplet in 2D.

Theorem 6 (*2D local attenuation and 2D local phase*)**.** *Let f be a 1D function in $\mathbb{L}_1$ such that its 1D analytic scale-space representation has no zeros in the plane $s > 0$ and let $\mathbf{n} \in \mathbb{R}^2$ with $|\mathbf{n}| = 1$. Furthermore, let $u(\mathbf{x}; s)$ be the 2D scale-space representation of $f(\mathbf{n}\cdot\mathbf{x})$ and let $\mathbf{v}(\mathbf{x}; s)$ be the corresponding image flux. Then the local attenuation* (20) *and the local phase-vector* (15) *form a Riesz triplet*

$$\mathbf{r}(\mathbf{x}; s) = (\mathbf{h} * a(\cdot; s))(\mathbf{x}) \quad \textit{for all } s \geq 0. \tag{21}$$

Proof: Since $f(\mathbf{n}\cdot\mathbf{x})$ is constant in the perpendicular direction $\mathbf{n}^\perp$ of $\mathbf{n}$, we focus on the projections onto the plane spanned by $\mathbf{n}$ and s, i.e., integrals along $\mathbf{n}^\perp$. From the Fourier slice theorem [4] it follows that the 1D projections of the 2D Poisson kernel and the 2D Riesz kernel are identical to the 1D Poisson kernel and $\mathbf{n}$-times the Hilbert kernel, respectively:

$$\int_{-\infty}^{\infty} \frac{s}{2\pi(|x'\mathbf{n} + y'\mathbf{n}^\perp|^2 + s^2)^{3/2}}\, dy' = \frac{s}{\pi(x'^2 + s^2)} \tag{22}$$

$$\int_{-\infty}^{\infty} \frac{x'\mathbf{n} + y'\mathbf{n}^\perp}{2\pi|x'\mathbf{n} + y'\mathbf{n}^\perp|^3}\, dy' = \frac{\mathbf{n}}{\pi x'}, \tag{23}$$

where we made use of $\mathbf{x} = x'\mathbf{n} + y'\mathbf{n}^\perp$. Thus, all 2D convolutions of $f(\mathbf{n}\cdot\mathbf{x})$ with either the Poisson kernel or the Riesz kernel can be replaced with 1D

convolutions with the 1D Poisson kernel and **n**-times the Hilbert kernel. Hence, $u(\mathbf{x}; s) = u_1(\mathbf{n} \cdot \mathbf{x}; s)$ and $\mathbf{v}(\mathbf{x}; s) = \mathbf{n} v_1(\mathbf{n} \cdot \mathbf{x}; s)$, where $u_1 + i v_1$ denotes the 1D analytic scale-space of f. Therefore, making use of (20) and (15) we obtain

$$a(\mathbf{x}; s) = a_1(\mathbf{n} \cdot \mathbf{x}; s) \quad \text{and} \quad \mathbf{r}(\mathbf{x}; s) = \mathbf{n} r_1(\mathbf{n} \cdot \mathbf{x}; s)$$

where $a_1 = \log |u_1 + i v_1|$ is the 1D attenuation and $r_1 = \arg(u_1 + i v_1)$ is the 1D phase.[14] Since r_1 is the Hilbert transform of a_1, we obtain (21) by applying (23). □

Before we focus on the problem of zeros in the positive half-space, we want to make some remarks.

1. The 2D signals which occur in Theorem 6 are globally intrinsically 1D, compare Definition 6.
2. Although real images are in general not globally intrinsically 1D signals, they commonly contain a lot of intrinsically 1D neighborhoods. In these regions, Theorem 6 can be considered to provide an approximative result, since the Poisson kernel and the Riesz kernel are rapidly decreasing with increasing radius such that the error caused by a finite integration (projection) is small.
3. For intrinsically 2D neighborhoods the theorem does not hold in general.
4. As we will see further below, one can apply the 2D attenuation-phase relationship in good approximation neglecting possibly occurring zeros.

Note that all subsequent examples are computed using a finite domain implementation of the monogenic scale-space [16], since the boundary effects, which occur if convolution operators are applied to finite images, yield quite large distortions.

In theory, Theorem 6 cannot be applied to most images, since zeros are occurring in the positive half-space in most cases, see Fig. 10. However, in practical applications the influence of the zeros can mostly be neglected, as we see from two very simple reconstruction algorithms which make use of Theorem 6: reconstruction from local attenuation and reconstruction from local phase-vector. The reconstruction works as follows.

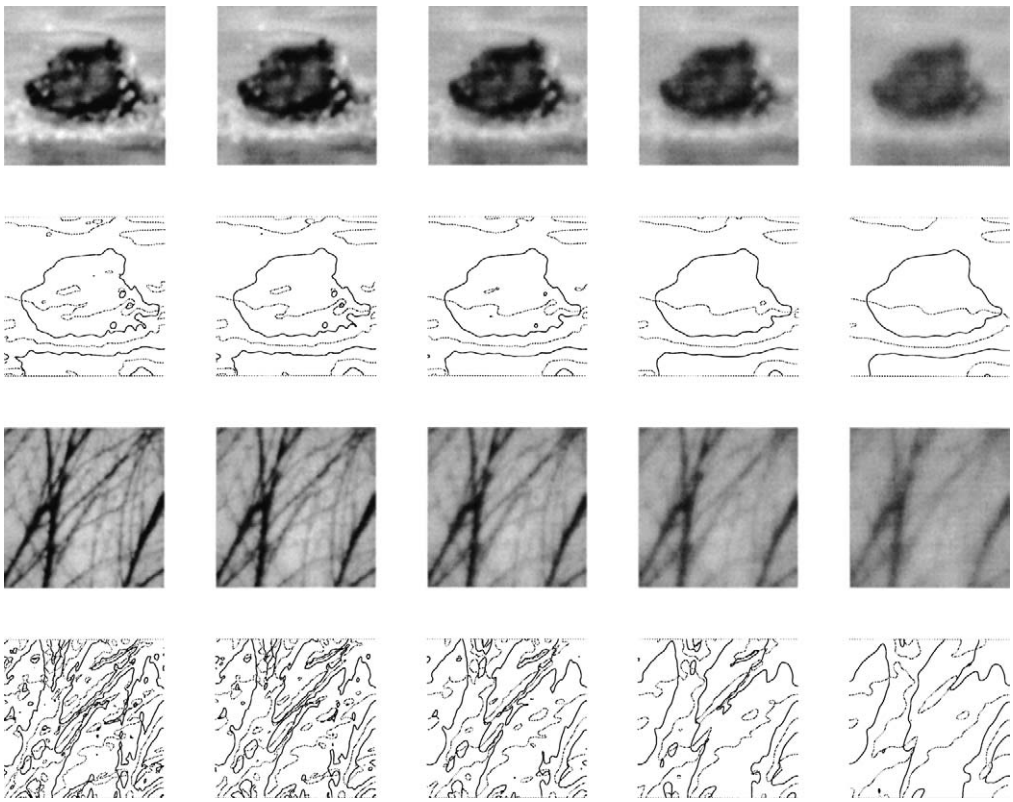

Figure 10. Zeros in the monogenic scale-space for two different images (see Fig. 11) and a range of scales. The black lines show the zeros of the Poisson scale-space and the gray lines show the zeros of the figure flow. The intersections of both are the zeros of the monogenic scale-space.

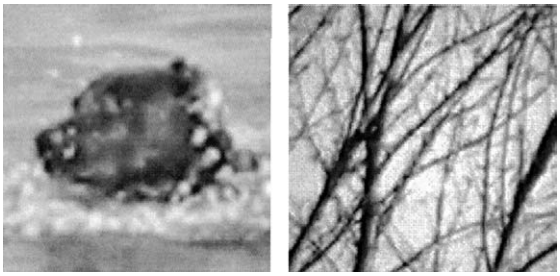

Figure 11. Two test images.

From (20) and (15) it follows that the signal at scale s_0 can be recovered from attenuation and phase-vector by

$$u(\mathbf{x}; s_0) = \exp(a(\mathbf{x}; s_0)) \cos(|\mathbf{r}(\mathbf{x}; s_0)|). \tag{24}$$

Assuming that only either feature, attenuation or phase-vector, is known, the respective other one can be computed using (21).[15] Hence, we obtain methods for reconstruction from local phase-vector and local attenuation, respectively.

We applied the two methods to the images in Fig. 11. The results can be found in Fig. 12. The reconstructed images (especially those reconstructed from the phase-vector) might have a different dynamics and a DC-offset. In order to have a fair comparison, we minimized the mean square error of the reconstruction with respect to a global multiplicative constant and an additive offset. The resulting RMSEs[16] can be found in Table 2.

Table 2. RMSEs of the reconstructed images.

Image/ method	Dog/phase	Dog/ attenuation	Tree/ phase	Tree/ attenuation
RMSE	9.15	4.17	10.50	4.38

The reconstruction results are quite accurate (see footnote 16) which implies that the influence of existing zeros in the monogenic scale-space is comparably low. Obviously, the reconstruction accuracy is better for the reconstruction from local attenuation. Especially close to the boundary the error of the reconstruction from phase is significantly larger. This is probably caused by the finite domain implementation, which constraints the normal components of the Riesz transform to vanish at the boundary [16].

To conclude this section, we want to make a final remark on Theorem 6. In [18] we have stressed the fact that local amplitude and local phase are independent information. This statement must be restated in an exacter way in the current context: local amplitude and local phase are *pointwise* independent. In a local context, local attenuation and local phase-vector are related by the Riesz transform. Hence, the framework of the monogenic scale-space represents local relationships explicitly in pointwise orthogonal features.

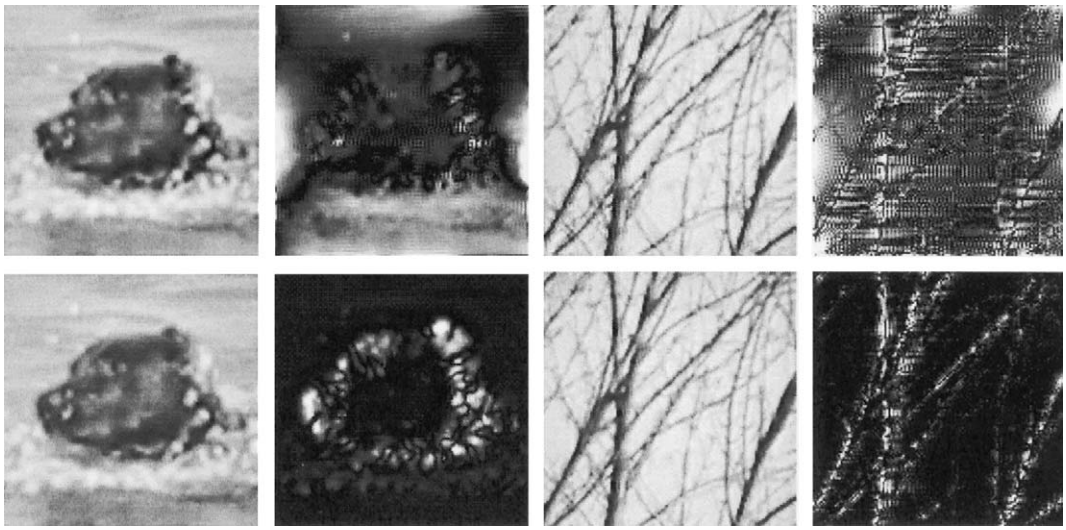

Figure 12. Reconstruction from attenuation and phase. Upper row: reconstruction from local phase. Bottom row: reconstruction from local amplitude. The pairwise left images show the reconstruction, the pairwise right ones the corresponding absolute error multiplied by 10.

3.4. *Phase-Based and Amplitude-Based Image Processing*

The theorems and observations from the previous sections enable us to relate phase-based image processing approaches to amplitude-based approaches on a theoretic level. In order to obtain exact results, we have to assume that there are no zeros in the monogenic scale-space for $s > 0$, although this assumption can be omitted in most practical situations.

Under the assumptions of Theorem 6, the local attenuation and the local phase-vector form a monogenic function for $s > 0$. Accordingly, we can apply (9) and (10) to relate the first order derivatives of the local attenuation and those of the local phase-vector:

$$\nabla_2 \cdot \mathbf{r}(\mathbf{x}; s) + \partial_s a(\mathbf{x}; s) = 0 \tag{25}$$

$$\partial_s \mathbf{r}(\mathbf{x}; s) - \nabla_2 a(\mathbf{x}; s) = 0. \tag{26}$$

Furthermore, (8) implies that the phase-vector field is irrotational. This is trivially fulfilled in intrinsically 1D neighborhoods, but (8) can also be considered as a criterion for the validity of (25) and (26).

Both Eqs. (25) and (26) contain quite fundamental terms of image processing: the (isotropic) *local frequency* $\nabla_2 \cdot \mathbf{r}(\mathbf{x}; s)$ and the differential phase congruency $\partial_s \mathbf{r}(\mathbf{x}; s)$. These observations give rise to two theorems.

Theorem 7 (*local frequency*)**.** *The local frequency in an intrinsically* 1*D neighborhood is given by the scale derivative of the local attenuation.*

Theorem 8 (*phase congruency*)**.** *The phase congruency in an intrinsically* 1*D neighborhood is given by the extrema of the local amplitude.*

Proof of Theorem 7: In the first part we show that in the case of intrinsically 1D neighborhoods the isotropic local frequency is identical to the local frequency in the main orientation (see also [14]). Let $\mathbf{n} = (n_1, n_2)^T$ be the unit vector pointing in the main orientation. The local frequency in the main orientation is given by the directional derivative of the scalar phase φ: $\varphi' = (n_1\partial_x + n_2\partial_y)\varphi$. Since the neighborhood is intrinsically 1D, we know that $\nabla_2\varphi = \mathbf{n}\varphi'$ and because $\mathbf{r} = \mathbf{n}\varphi$,

$$\nabla_2 \cdot \mathbf{r}(\mathbf{x}; s)) = \mathbf{n} \cdot \nabla_2\varphi(\mathbf{x}; s) = \mathbf{n} \cdot \mathbf{n}\varphi'(\mathbf{x}; s) = \varphi'(\mathbf{x}; s).$$

In a second step, we show that (25) is fulfilled. Although it already follows from Theorem 6, we give an elementary proof here. Similar to [32], p. 397, we express the derivative of the local phase-vector directly by partial derivatives of the components of the monogenic scale-space (see also [14]):

$$\begin{aligned}
&\nabla_2 \cdot \mathbf{r}(\mathbf{x}; s) \\
&\quad = \frac{\mathbf{v}(\mathbf{x}; s)}{|\mathbf{v}(\mathbf{x}; s)|} \cdot \nabla_2 \arctan\left(\frac{|\mathbf{v}(\mathbf{x}; s)|}{u(\mathbf{x}; s)}\right) \\
&\quad = \frac{u(\mathbf{x}; s)(\nabla_2 \cdot \mathbf{v}(\mathbf{x}; s)) - \mathbf{v}(\mathbf{x}; s) \cdot (\nabla_2 u(\mathbf{x}; s))}{u(\mathbf{x}; s)^2 + |\mathbf{v}(\mathbf{x}; s)|^2},
\end{aligned}$$

where we made use of the local orientation being constant (intrinsically 1D neighborhood). By means of (9) and (10) we replace the spatial derivatives with a scale derivative:

$$\nabla_2 \cdot \mathbf{r}(\mathbf{x}; s) = -\frac{u(\mathbf{x}; s)(\partial_s u(\mathbf{x}; s)) + \mathbf{v}(\mathbf{x}; s) \cdot (\partial_s \mathbf{v}(\mathbf{x}; s))}{u(\mathbf{x}; s)^2 + |\mathbf{v}(\mathbf{x}; s)|^2}.$$

On the other hand, by (25) we have

$$\begin{aligned}
\partial_s a(\mathbf{x}; s) &= \frac{1}{2}\partial_s \log(u(\mathbf{x}; s)^2 + |\mathbf{v}(\mathbf{x}; s)|^2) \\
&= \frac{u(\mathbf{x}; s)(\partial_s u(\mathbf{x}; s)) + \mathbf{v}(\mathbf{x}; s) \cdot (\partial_s \mathbf{v}(\mathbf{x}; s))}{u(\mathbf{x}; s)^2 + |\mathbf{v}(\mathbf{x}; s)|^2}.
\end{aligned}$$

□

Theorem 7 formalizes a well known method: The isotropic local frequency can be estimated by the quotient of two log-normal bandpass filters (see e.g. [32]). The latter can be considered as a finite difference of frequency components at two different scales, i.e., an approximation of the scale derivative.

Proof of Theorem 8: By Theorem 4 we know that the scale derivative of the phase can be expressed by means of scale derivatives of the components of the monogenic scale-space. Furthermore,

$$\begin{aligned}
\nabla_2 a(\mathbf{x}; s) &= \frac{1}{2}\nabla_2 \log(u(\mathbf{x}; s)^2 + |\mathbf{v}(\mathbf{x}; s)|^2) \\
&= \frac{u(\mathbf{x}; s)(\nabla_2 u(\mathbf{x}; s)) + \mathbf{v}(\mathbf{x}; s)(\nabla_2 \cdot \mathbf{v}(\mathbf{x}; s))}{u(\mathbf{x}; s)^2 + |\mathbf{v}(\mathbf{x}; s)|^2}
\end{aligned}$$

and plugging in (10) and (9) yields

$$\nabla_2 a(\mathbf{x}; s) = \frac{u(\mathbf{x}; s)\partial_s \mathbf{v}(\mathbf{x}; s) - \mathbf{v}(\mathbf{x}; s)\partial_s u(\mathbf{x}; s)}{u(\mathbf{x}; s)^2 + |\mathbf{v}(\mathbf{x}; s)|^2}.$$

Hence, points of phase congruency are identical to points of vanishing gradient of the attenuation. Since

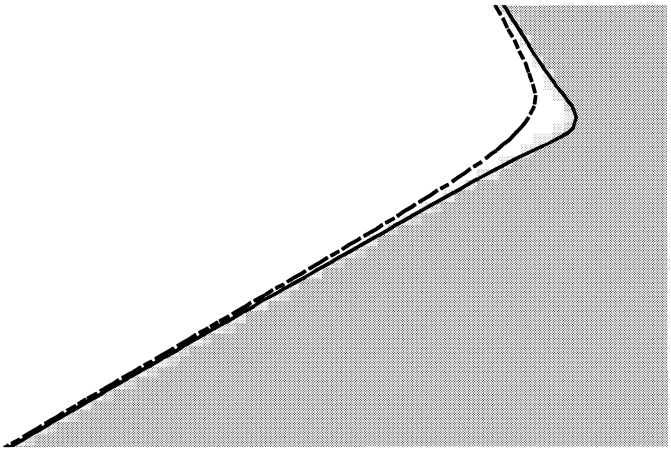

Figure 13. Edge detection at synthetic corner. Solid: zero-crossing of phase congruency, dashed: zero-crossing of amplitude gradient.

the exponential function is strict monotonic, a vanishing gradient of the attenuation implies a vanishing gradient of the amplitude.

What remains is to show that only extrema of the amplitude correspond to points of phase congruency. Assuming that we have a zero gradient and no extremum, implies that $\Delta_2 a = 0$ and due to (26) $\partial_{ss}\,\mathbf{r} = 0$. However, this case is excluded by applying any non-zero threshold (see Section 3.1) to the slope of the zero. □

Note that we apply the threshold only to the numerator in (17), such that the slope of the zero is implicitly multiplied with the squared amplitude. Hence, for an appropriate threshold, this method also excludes local minima. In other words: edge detection by means of local amplitude maxima is equivalent to edge detection by phase congruency.

This result is just contrary to looking at phase based and amplitude based approaches as being two alternative approaches (see e.g. [34]). In order to solve this contradiction of established opinions, we concentrate on an assumption made in the beginning: What happens if the neighborhood is not intrinsically 1D? We cannot give an exhaustive answer to this question in this paper, since the behavior of phase and attenuation in intrinsically 2D neighborhoods is still work in progress. However, we present a simple example, consisting of a synthetic orthogonal corner, which shows that the phase congruency is superior to the detection of local amplitude maxima, see Fig. 13.

Obviously, the zero-crossing of the phase congruency is well located, even at the corner. Far away from the corner, the zero-crossing of the amplitude gradient looks quite similar, but close to the corner its localization is much poorer. Both methods are evaluated at the same scale ($s = 2$).

Hence, the main difference between approaches using the detection of local amplitude maxima and phase congruency approaches is the behavior in 2D neighborhoods. This can also be verified in various edge-detection experiments in [15], where the amplitude based approaches blur the contour at corners and junctions.

4. Conclusion

In this paper we have presented a unifying approach to scale-space theory and phase-based image processing. We combined the concept of the Poisson scale-space with the monogenic signal yielding the monogenic scale-space, which contains the scale-space and its flux, the Riesz transform. By means of the central Theorem 6 we established a relationship between the main features of the monogenic scale-space, the local attenuation and the local phase. The resulting theoretic framework yields several further relationships which can be exploited for image processing. However, the structure of the monogenic scale-space representation still needs further investigation to be completely understood.

Appendix

Why is Iijimas Original Uniqueness Proof Wrong?

In his paper [30] (in Japanese, a journal version of [29]), Iijima shows for the 1D case that the axioms

A1–A5[17] have a unique solution, the Gaussian scale-space. Besides the fact that he does not assure that the signal is continuously embedded, his proof must obviously contain an error, since the Poisson scale-space is a counterexample for his proof. The question is now, where exactly in the proof Iijima made the mistake.

It turns out that he introduced an assumption in the proof, which is not contained in the axioms. We skip the first three steps of his proof, which make use of the first three axioms in order to show that the observation transformation must have the following form (see also Lemma 3 in [50]):

$$\Phi[g(x'), x, \sigma] = \int_{-\infty}^{\infty} g(x')\phi(v(\sigma)(x - x'))v(\sigma)\, dx',$$

where we use the notation from [50], which is basically the same as the original one.

In a next step, using axiom A4, Iijima shows that the Fourier transform of the kernel $\phi(u)$ must be an exponential function with even exponent, which excludes the Poisson scale-space and all valid solutions according to [11, 42], see also Lemma 4 in [50]. Hence, the error must be in this fourth part of the proof.

Indeed, Iijima assumes in [30], p. 373, that the first n derivatives of the frequency response $\Psi(\xi)$ of the scale-space kernel do exist at the origin (Eq. (3.10)). In the axioms, however, no constraints are put on the frequency response (it is not even assumed that the observation transformation is connected to a frequency response at all). Replacing the derivatives at the origin with left-sided and right-sided limits, i.e., allowing a singularity of the derivative at the origin, splits the inverse Fourier transform in (3.13) into two addends (using the original notation):

$$\phi(u) = \frac{1}{2\pi}\left(\int_{-\infty}^{0} \exp\left(\lim_{\tau\uparrow 0} \Psi^{(n)}(\tau)\frac{\xi^n}{n!} + i\xi u \right) d\xi + \int_{0}^{\infty} \exp\left(\lim_{\tau\downarrow 0} \Psi^{(n)}(\tau)\frac{\xi^n}{n!} + i\xi u \right) d\xi \right).$$

This sum of integrals does not only exist for $n = 2m$ (m an integer) as stated in the original proof. In particular, the Poisson kernel ($n = 1$) is also a solution which can easily be verified.

In a fifth step, Iijima shows that the positivity is only preserved if $m \leq 1$, see also [11].[18] If $n = 2m$ had been correct, the Gaussian kernel would have been the only solution. However, changing the proof as indicated above results in two solutions for linear scale-space kernels ($n = 1$ and $n = 2$). The remaining solutions according to [42, 12] ($K_t(u) = \exp(-2\pi|u|^\alpha t$, $\alpha \in (0, 2]$) cannot be obtained by a proof similar to the one by Iijima, since he uses explicitly the inverse Fourier transform which does only exist for certain values of α [42] and which is actually a further implicit assumption.

Uncertainty of the 2D Poisson Kernel

The spread in the spatial domain reads (see [15])

$$\begin{aligned}\Delta\mathbf{x} = \sqrt{\sigma_{\mathbf{x}}^2} &= \left(\frac{\iint |\mathbf{x}|^2 p(\mathbf{x}; s)^2\, dx\, dy}{\iint p(\mathbf{x}; s)^2\, dx\, dy} \right)^{1/2} \\ &= \left(\frac{\iint \frac{|\mathbf{x}|^2}{(|\mathbf{x}|^2+s^2)^3}\, dx\, dy}{\iint \frac{1}{(|\mathbf{x}|^2+s^2)^3}\, dx\, dy} \right)^{1/2} \\ &\quad \text{change to polar coordinates } r = |\mathbf{x}|\text{:} \\ &= \left(\frac{2\pi \int_0^\infty \frac{r^3}{(r^2+s^2)^3}\, dr}{2\pi \int_0^\infty \frac{r}{(r^2+s^2)^3}\, dr} \right)^{1/2} = \left(\frac{\frac{1}{2s^2} - \frac{s^2}{4s^4}}{\frac{1}{4s^4}} \right)^{1/2} = s\end{aligned}$$

where the integrals are evaluated according to [6] 19.5.1.3 integrals 63 and 71. The spread in the frequency domain is obtained as

$$\begin{aligned}\Delta\boldsymbol{\xi} = \sqrt{\sigma_{\boldsymbol{\xi}}^2} &= \left(\frac{\iint |\boldsymbol{\xi}|^2 P(\boldsymbol{\xi}; s)^2\, d\xi\, d\eta}{\iint P(\boldsymbol{\xi}; s)^2\, d\xi\, d\eta} \right)^{1/2} \\ &= \left(\frac{\iint |\boldsymbol{\xi}|^2 \exp(-4\pi|\boldsymbol{\xi}|s)\, d\xi\, d\eta}{\iint \exp(-4\pi|\boldsymbol{\xi}|s)\, d\xi\, d\eta} \right)^{1/2} \\ &\quad \text{change to polar coordinates } q = |\boldsymbol{\xi}|\text{:} \\ &= \left(\frac{2\pi \int_0^\infty q^3 \exp(-4\pi qs)\, dq}{2\pi \int_o^\infty q \exp(-4\pi qs)\, dq} \right)^{1/2} \\ &= \left(\frac{\frac{6}{(4\pi s)^4}}{\frac{1}{(4\pi s)^2}} \right)^{1/2} = \frac{\sqrt{6}}{4\pi s}\end{aligned}$$

where the integrals are evaluated according to [6] 19.6.1 integral 1. Hence $(\Delta\mathbf{x})(\Delta\boldsymbol{\xi}) = \frac{\sqrt{6}}{4\pi}$ in the case of the Poisson kernel which means that the uncertainty is slightly worse than for the 2D Gaussian kernel (factor $\sqrt{1.5}$).

Acknowledgments

We appreciate the help of Nils Madeja for translating parts of [29] for finding the error in the original proof. Furthermore, we like to thank Remco Duits and Luc Florack for intensive discussions on the axiomatics of linear scale-space in context of the Poisson scale-space.

Notes

1. Since we are interested in scale-space axiomatics for image processing, we only consider formulations for 2D signals. Note that we use the notion of 2D scale-space, although the scale-space representation is a 3D function.
2. Originally, Iijima formulated the 2D axiomatic for the affine case, i.e., the blurring parameter is a matrix Σ. In this paper however, we focus on a scalar scale parameter, since adaptive or very high dimensional scale-spaces (a blurring parameter Σ has three degrees of freedom) are out of the scope of this paper.
3. We use the term 'scale and rotation invariant linear scale-space' in order to distinguish it clearly from the definitions of linear scale-space according to the ideas of information reduction. In the following we will omit 'scale and orientation invariant' if it is clear from the context which scale-space we mean.
4. We explicitly distinguish between the causality requirement (axiom A8) and the non-enhancement, since the informal definition of causality is slightly weaker than the convexity constrain (see Section 2.3).
5. Actually, the Poisson scale-space is not new: In [42] Pauwels et al. have considered a class of scale-space kernels, among which they also mentioned explicitly the 1D Poisson kernel (Cauchy density). In our two conference papers [19, 21], the Poisson kernel already appeared in the context of scale-space, which was further discussed in [15]. Independently, Duits et al. started investigations about scale-space axiomatics, first results can be found in [11, 12].
6. Actually the constant $-(4\pi)^{-1}$ is an arbitrary choice, any other constant is a valid choice [7], p. 209. However, due to normalization of the Dirac impulse, we prefer the given constant.
7. Any gradient field (e.g. the figure flow according to Fick's law) fulfills (8).
8. We avoid using the term '2D analytic signal', since the 1D analytic signal is derived from a 2D analytic function [26] (which is indeed the analytic Poisson scale-space, see below) and the approaches commonly referred to as '2D analytic signals' are just projections of the 1D approach, i.e., they are not derived from a concept of a higher dimensional analytic function.
9. One consequence is that the image intensity axis is identified with the scale axis [15].
10. For discrete signals, the non-enhancement is also fulfilled for other kernels [38].
11. The proof of Hummel cannot be directly applied to the Poisson scale-space, since the maximum principle is different in both cases.
12. A minimum-phase system is defined by having no zeros and poles in the positive half-plane of the Laplace domain.
13. Due to the maximum principle, we know that no poles occur for $s > 0$.
14. Note that $\arg(u + iv) = \frac{v}{|v|} \arctan(\frac{|v|}{u})$ if $\arctan(\cdot) \in [0, \pi)$.
15. Note that the inverse Riesz transform is given by the negative Riesz transform, as for the Hilbert transform.
16. Note that RMSEs are in gray level units, i.e., they are not normalized. Taking the normalized MSEs instead, we obtain errors of order 10^{-3} (reconstruction from local phase) and 10^{-4} (reconstruction from local attenuation), which is quite good compared to other methods, see e.g. [2].
17. Axiom A4 becomes even simpler in 1D, since it just requires scale invariance.
18. Originally, A5 was no axiom, but an additional constraint.

References

1. J. Babaud, A.P. Witkin, M. Baudin, and R.O. Duda, "Uniqueness of the Gaussian kernel for scale-space filtering," *IEEE Transactions on Pattern Analysis and Machine Intelligence*, Vol. 8, No. 1, pp. 26–33, 1986.
2. J. Behar, M. Porat, and Y.Y. Zeevi. "Image reconstruction from localized phase," *IEEE Transactions on Signal Processing*, Vol. 40, No. 4, pp. 736–743, 1992.
3. R.N. Bracewell, *The Fourier Transform and its Applications*, McGraw Hill, 1986.
4. R.N. Bracewell, *Two-Dimensional Imaging*, Prentice Hall Signal Processing Series. Prentice Hall, Englewood Cliffs, 1995.
5. F. Brackx, R. Delanghe, and F. Sommen, *Clifford Analysis*, Pitman: Boston, 1982.
6. I. Bronstein, K. Semendjajew, G. Musiol, and H. Mühlig, *Taschenbuch der Mathematik*, Verlag Harri Deutsch, Frankfurt, 1993.
7. K. Burg, H. Haf, and F. Wille, *Höhere Mathematik für Ingenieure, Band V Funktionalanalysis und Partielle Differentialgleichungen*, Teubner Stuttgart, 1993.
8. K. Burg, H. Haf, and F. Wille, *Höhere Mathematik für Ingenieure, Band IV Vektoranalysis und Funktionentheorie*, Teubner Stuttgart, 1994.
9. P.J. Burt and E.H. Adelson, "The Laplacian pyramid as a compact image code," *IEEE Trans. Communications*, Vol. 31, No. 4, pp. 532–540, 1983.
10. F. Catté, P.-L. Lions, J.-M. Morel, and T. Coll, "Image selective smoothing and edge detection by nonlinear diffusion," *SIAM J. Numer. Analysis*, Vol. 32, pp. 1895–1909, 1992.
11. R. Duits, L.M.J. Florack, J. de Graaf, and B.M. ter Haar Romeny, "On the axioms of scale space theory," *Journal of Mathematical Imaging and Vision*, 2002 (accepted).
12. R. Duits, L.M.J. Florack, B. M. ter Haar Romeny, and J. de Graaf, "Scale-space axioms critically revisited," in *Signal and Image Processing*, N. Younan (Ed.), IASTED, ACTA Press, Kauai, August 2002, pp. 304–309.
13. M. Evans, N. Hastings, and J.B. Peacock, *Statistical Distributions*, 3rd. ed., Wiley-Interscience, 2000.
14. M. Felsberg, "Disparity from monogenic phase," in *24. DAGM Symposium Mustererkennung, Zürich*, L.V. Gool (Ed.), Vol. 2449 of Lecture Notes in Computer Science, Springer, Heidelberg, 2002, pp. 248–256.
15. M. Felsberg, *Low-Level Image Processing with the Structure Multivector*, Ph.D. thesis, Institute of Computer Science and Applied Mathematics, Christian-Albrechts-University of Kiel, 2002. TR no. 0203, available at http://www.informatik.uni-kiel.de/reports/2002/0203.html.
16. M. Felsberg, R. Duits, and L. Florack, "The monogenic scale space on a bounded domain and its applications," in *Scale Space Conference*, 2003 (accepted).
17. M. Felsberg and G. Sommer, "A new extension of linear signal processing for estimating local properties and detecting features," in *22. DAGM Symposium Mustererkennung*, G. Sommer,

N. Krüger, and C. Perwass (Eds.), Springer, Heidelberg, Kiel, 2000, pp. 195–202.
18. M. Felsberg and G. Sommer, "The monogenic signal," *IEEE Transactions on Signal Processing*, Vol. 49, No. 12, pp. 3136–3144, 2001.
19. M. Felsberg and G. Sommer, "Scale adaptive filtering derived from the Laplace equation," in *23. DAGM Symposium Mustererkennung*, B. Radig and S. Florczyk (Eds.), Vol. 2191 of Lecture Notes in Computer Science, Springer, Heidelberg, München, 2001, pp. 124–131.
20. M. Felsberg and G. Sommer, "The Poisson scale-space: A unified approach to phase-based image processing in scale-space," Tech. Rep. LiTH-ISY-R-2453, Dept. EE, Linköping University, SE-581 83 Linköping, Sweden, 2002.
21. M. Felsberg and G. Sommer, "The structure multivector," in *Applied Geometrical Algebras in Computer Science and Engineering*, Birkhäuser, Boston, 2002, pp. 437–448.
22. L. Florack, *Image Structure*, Vol. 10 of *Computational Imaging and Vision*, Kluwer Academic Publishers, 1997.
23. L. Florack and A. Kuijper, "The topological structure of scale-space images," *Journal of Mathematical Imaging and Vision*, Vol. 12, No. 1, pp. 65–79, 2000.
24. G.H. Granlund, "In search of a general picture processing operator," *Computer Graphics and Image Processing*, Vol. 8, pp. 155–173, 1978.
25. G.H. Granlund and H. Knutsson, *Signal Processing for Computer Vision*, Kluwer Academic Publishers: Dordrecht, 1995.
26. S.L. Hahn, *Hilbert Transforms in Signal Processing*, Artech House: Boston, London, 1996.
27. D. Hestenes, "Multivector calculus," *J. Math. Anal. and Appl.*, Vol. 24, No. 2, pp. 313–325, 1968.
28. R.A. Hummel, "Representations based on zero-crossings in scale space," in *Proc. IEEE Comp. Soc. Conf. Computer Vision and Pattern Recognition*, Miami Beach, 1986, pp. 204–209.
29. T. Iijima, "Basic theory of pattern observation," in *Papers of Technical Group on Automata and Automatic Control, IECE, Japan*, December 1959.
30. T. Iijima, "Basic theory on normalization of pattern (In case of a typical one-dimensional pattern)," *Bulletin of the Electrotechnical Laboratory*, Vol. 26, pp. 368–388, 1962.
31. T. Iijima, "Observation theory of two-dimensional visual patterns," in *Papers of Technical Group on Automata and Automatic Control, IECE, Japan*, October 1962.
32. B. Jähne, *Digitale Bildverarbeitung*, Springer: Berlin, 1997.
33. J.J. Koenderink, "The structure of images," *Biological Cybernetics*, Vol. 50, pp. 363–370, 1984.
34. P. Kovesi, "Image features from phase information," *Videre: Journal of Computer Vision Research*, Vol. 1, No. 3, 1999.
35. S.G. Krantz, *Handbook of Complex Variables*, Birkhäuser: Boston, 1999.
36. G. Krieger and C. Zetzsche, "Nonlinear image operators for the evaluation of local intrinsic dimensionality," *IEEE Transactions on Image Processing*, Vol. 5, No. 6, pp. 1026–1041, 1996.
37. T. Lindeberg, *Scale-Space Theory in Computer Vision*, The Kluwer International Series in Engineering and Computer Science. Kluwer Academic Publishers: Boston, 1994.
38. T. Lindeberg, "Linear spatio-temporal scale-space," in *Scale-Space Theory in Computer Vision*, Vol. 1252 of Lecture Notes in Computer Science, Springer: Utrecht, Netherlands, 1997.
39. T. Lindeberg, *On the Axiomatic Foundations of Linear Scale-Space: Combining Semi-Group Structure with Causality vs. Scale Invariance*, Ch. 6, Kluwer Academic, 1997.
40. A. Papoulis, *The Fourier Integral and its Applications*, McGraw-Hill: New York, 1962.
41. A. Papoulis, *Probability, Random Variables and Stochastic Processes*, McGraw-Hill, 1965.
42. E.J. Pauwels, L.J. Van Gool, P. Fiddelaers, and T. Moons, "An extended class of scale-invariant and recursive scale space filters," *IEEE Transactions on Pattern Analysis and Machine Intelligence*, Vol. 17, No. 7, pp. 691–701, 1995.
43. P. Perona and J. Malik, "Scale-space and edge detection using anisotropic diffusion," *IEEE Trans. Pattern Analysis and Machine Intelligence*, Vol. 12, No. 7, pp. 629–639, 1990.
44. D. Reisfeld, "The constrained phase congruency feature detector: Simultaneous localization, classification and scale determination," *Pattern Recognition Letters*, Vol. 17, pp. 1161–1169, 1996.
45. J.L. Schiff, *The Laplace Transform*, Undergraduate Texts in Mathematics. Springer: New York, 1999.
46. N. Sochen, R. Kimmel, and R. Malladi, "A geometrical framework for low level vision," *IEEE Trans. on Image Processing, Special Issue on PDE Based Image Processing*, Vol. 7, No. 3, pp. 310–318, 1998.
47. E. Stein and G. Weiss, *Introduction to Fourier Analysis on Euclidean Spaces*, Princeton University Press: New Jersey, 1971.
48. J. Weickert, "Anisotropic siffusion in image processing," Ph.D. thesis, Faculty of Mathematics, University of Kaiserslautern, 1996.
49. J. Weickert, "A review of nonlinear diffusion filtering," in *Scale-Space Theory in Computer Vision*, B. ter Haar Romeny, L. Florack, J. Koenderink, and M. Viergever (Eds.), Vol. 1252 of LNCS, Springer: Berlin, 1997, pp. 260–271.
50. J. Weickert, S. Ishikawa, and A. Imiya, "Scale-space has first been proposed in Japan," *Mathematical Imaging and Vision*, Vol. 10, pp. 237–252, 1999.
51. A.P. Witkin, "Scale-space filtering," in *Proc. 8th Int. Joint Conf. Art. Intell.*, 1983, pp. 1019–1022.
52. A.L. Yuille and T. Poggio, "Scaling theorems for zero-crossings," *IEEE Trans. Pattern Analysis and Machine Intell.*, Vol. 8, pp. 15–25, 1986.

Michael Felsberg received a diploma degree in engineering from Christian-Albrechts-University Kiel, Germany, in 1998. During his

Ph.D. studies at the Cognitive Systems Group in Kiel he hold scholarships from the DFG Graduiertenkolleg No. 357. and the German National Merit Foundation (Studienstiftung des Deutschen Volkes). He received his Ph.D. degree in engineering (summa cum laude) from Kiel University in 2002. His research interests include multidimensional signal theory, image processing, and low level computer vision by means of advanced algebraic methods and signal representations.

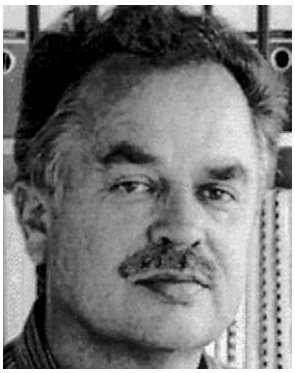

Gerald Sommer received a diploma degree in physics from Friedrich-Schiller-University Jena, Germany, in 1969, a Ph.D. degree in physics from the same university in 1975, and a habilitation degree in engineering from Technical University Ilmenau, Germany, in 1988. From 1969 to 1991 he worked at several departments of the Friedrich-Schiller-University Jena. From 1991 to 1993 he was the head of the division for medical image processing at the Research Center for Environment and Health (GSF-Medis) in Munich-Neuherberg. Since 1993 he is professor for computer science at the Christian-Albrechts-University Kiel. He is leading the research group cognitive systems. Contemporary, his main interests are the design of behavior based systems. The research covers signal theory and signal processing, neural computation for pattern recognition, computer vision, and robot control.